

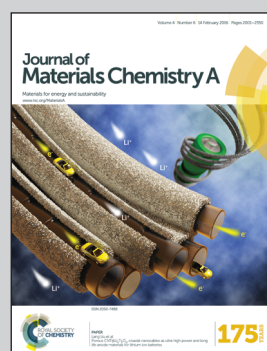


Showcasing a study on the fabrication of hybrid carbon-encapsulated hollow manganese oxide nanotubes with a porous-wall structure by Dr. Jung Inn Sohn at the University of Oxford and Prof. Hyo-Jin Ahn at Seoul National University of Science and Technology.

Title: Hierarchical architecture of hybrid carbon-encapsulated hollow manganese oxide nanotubes with a porous-wall structure for high-performance electrochemical energy storage

Novel hybrid carbon-encapsulated porous hollow manganese oxide nanotubes give synergistic effects on structural stability, allowing for superior cycling performance, because in addition to the void space between the porous walls, they provide additional internal void space to sufficiently accommodate volume expansion and contraction during the cycling.

As featured in:



See Jung Inn Sohn,
Hyo-Jin Ahn et al.,
J. Mater. Chem. A, 2016, 4, 2049.

COMMUNICATION

[View Article Online](#)
[View Journal](#) | [View Issue](#)



Cite this: *J. Mater. Chem. A*, 2016, 4, 2049

Received 9th December 2015
Accepted 23rd December 2015

DOI: 10.1039/c5ta10067d

www.rsc.org/MaterialsA

Hierarchical architecture of hybrid carbon-encapsulated hollow manganese oxide nanotubes with a porous-wall structure for high-performance electrochemical energy storage[†]

Geon-Hyoung An,^a Jung Inn Sohn^{*b} and Hyo-Jin Ahn^{*a}

Metal-oxide-based anode materials in energy storage devices continue to be of considerable interest for both fundamental science and potential technological applications because of their diverse functionalities, high theoretical capacity, cost-effectiveness, and non-polluting nature. However, despite these favourable features for various power source applications, important challenges associated with insertion-induced structural degradation remain, leading to capacity fading, and must be addressed to move towards the practical use of high-capacity metal oxide anodes. Here, we report the successful synthesis of novel hierarchical carbon-encapsulated manganese oxide architectures with hollow-tube structures and unique porous walls *via* a simple microwave process coupled with a hydrothermal method. This approach provides beneficial synergistic effects in terms of structural stability, electrochemical active surface areas, and electrical and ionic pathways. The carbon-encapsulated porous hollow manganese oxide nanotubes exhibit excellent electrochemical characteristics with large reversible specific capacity and excellent cycling stability (875 mA h g^{-1} capacity retention up to 100 cycles) as well as outstanding high-rate performance (729 mA h g^{-1} at 700 mA g^{-1}), which is the highest value thus far reported for manganese-oxide-based anode materials.

Recent technological advances in the rapidly emerging areas of portable electronic devices and electric vehicles have sparked significant research interests towards the development of high-performance power sources. In particular, Li-ion batteries (LIBs) have received considerable attention as one of the most promising energy storage devices because of their attractive features, such as high energy density, excellent cycling stability, no memory effect, low self-discharge rate, and environmental friendliness.^{1–5} However, to move Li-ion technology forward

towards genuine practical applications, further improvements of LIB anodes are crucial to satisfy the requirements of industrial applications; as a crucial component, the anodes play a paramount role in determining the battery weight, volume, cost effectiveness, and performance. Accordingly, based on the rational design and engineering of electrode materials, thus far, numerous strategies have been developed to improve the specific capacity of LIB anodes by introducing various transition metal dichalcogenides, alloy and composite materials including Si, metals, metal oxides as alternatives to conventional graphite with a low theoretical specific capacity of 372 mA h g^{-1} .^{6–11} Alternatively, other strategies have been developed to prevent severe volume-expansion-induced stress, which causes capacity fading during insertion/extraction cycling, through nano- and porous-structuring techniques or a combination of such techniques and carbon-based materials. These strategies allow anode materials to maintain their structural integrity and electrical conductivity.^{12–18} However, these approaches require relatively sophisticated schemes and techniques to control the internal void space in the structure to position engineered nanostructured materials within defined pores to accommodate volume expansion. Further development is necessary, particularly for high-capacity metal oxide materials, which have been widely considered to be promising anode materials for next-generation LIBs but suffer from significant difficulties in engineering the morphology and structure of the complicated oxides at the nanoscale.^{19,20} One of the most prominent challenges associated with metal oxide material processing is addressing the deterioration of the anode material properties that accompanies the structural volume expansion during cycling. Therefore, the development of a novel and simple strategy to effectively solve problems such as the large volume expansion and significant aggregation occurring during cycling as well as the high electrical conductivity is critical.

Herein, we report a novel architecture of carbon-encapsulated porous hollow nanotubes based on manganese oxide (C-PHNT) as a typical high-capacity metal oxide material fabricated using a simple hierarchical hybrid approach based on

^aDepartment of Materials Science and Engineering, Seoul National University of Science and Technology, Seoul 139-743, Korea. E-mail: hjahn@seoultech.ac.kr

^bDepartment of Engineering Science, University of Oxford, Oxford OX1 3PJ, UK. E-mail: junginn.sohn@eng.ox.ac.uk

[†] Electronic supplementary information (ESI) available. See DOI: 10.1039/c5ta10067d

a combination of a microwave process and hydrothermal method.

Fig. 1 schematically illustrates the synthetic route for fabricating C-PHNTs. First, we employed an electrospinning method to prepare carbon nanofibres (CNFs) as template materials (Fig. 1a) to produce hollow manganese oxide nanotubes, followed by a chemical precipitation method using an aqueous solution of KMnO_4 (Fig. 1b). Subsequently, the hollow nanotubes were then self-organized into hierarchical hollow nanotubes with a porous-wall structure using a microwave process, as demonstrated in Fig. 1c. Finally, the resultant porous hollow manganese oxide nanotubes (PHNTs) were further encapsulated by a carbon layer using a hydrothermal method. As a result, C-PHNTs with well-defined void spaces generated from the porous-wall and hollow-tube structures and capable of accommodating the volume expansion of manganese oxides were successfully prepared as anode materials for high-performance LIBs (Fig. 1d).

The geometrical and structural properties of the as-synthesized hierarchical structures were investigated using scanning electron microscopy (SEM), X-ray photoelectron spectroscopy (XPS), X-ray diffraction (XRD), and transmission electron microscopy (TEM). Fig. 2a presents the SEM images of the electrospun CNFs with diameters ranging from 213 to 229 nm, exhibiting round cross-sections and smooth surfaces. As expected, completely hollow manganese oxide nanotubes (Fig. 2b) were obtained through a chemical precipitation method involving the following redox reaction between CNFs and permanganate (MnO_4^-):^{21,22} $3\text{C} + 4\text{MnO}_4^- + \text{H}_2\text{O} = 4\text{MnO}_2 + 2\text{HCO}_3^- + \text{CO}_3^{2-}$. That is, the MnO_4^- was steadily reduced to MnO_2 by decomposing CNFs. XPS measurements (Fig. 2e) also confirmed that two different peaks observed at 642.7 eV and 653.9 eV correspond to the $\text{Mn } 2p_{3/2}$ and $\text{Mn } 2p_{1/2}$ peaks of the MnO_2 phases, respectively,²³ although no XRD signal was detected for the amorphous structure (Fig. S1†). During the microwave process, noticeably, we observed a considerable change in the surface morphology of the hollow manganese oxide nanotubes, leading to the formation of porous-wall structures from 400 °C, as observed in Fig. S2.† We obtained the

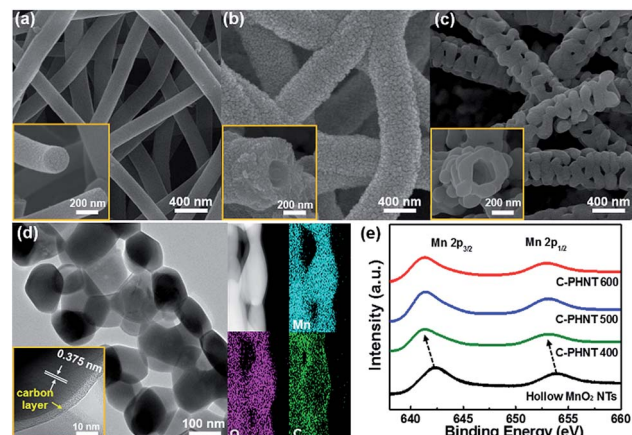


Fig. 2 Morphological and structural properties of the as-synthesized hierarchical structures. FESEM images of (a) CNFs, (b) hollow manganese oxide nanotubes, and (c) C-PHNT 600. (d) TEM image and EDS mapping data of C-PHNT 600. (e) XPS spectra of Mn 2p band shape.

optimized hollow nanotube structure with a well-defined porous-wall morphology at 600 °C (Fig. S2†), enabling effective accommodation of the volume change during the Li-ion insertion/extraction. In addition, the surface pore size increased with increasing microwave process temperatures; however, the one-dimensional structure of the hollow nanotubes almost collapsed at 700 °C (Fig. S2†). Then, because of carbonation through a hydrothermal process, individual PHNTs were entirely well encapsulated by carbon layers without any morphological changes (Fig. 2c and d), which could contribute not only to enhance the electrical conductivity and favourable ion diffusion but also to firmly maintain the entire hierarchical structure from a volume expansion. Carbon-encapsulated porous hollow manganese oxide nanotubes treated at 400 °C are referred to as “C-PHNT 400”. The uniform carbon layer with a thickness of approximately 3.9 nm was clearly identified by high-resolution TEM and energy-dispersive X-ray spectroscopy (EDS) as shown in Fig. 2d. Furthermore, the amount of carbon presence (0.93%) as a carbon encapsulation layer was determined by thermogravimetric analysis (TGA) measurements as shown in Fig. S3.† Notably, regardless of the microwave process temperatures, it was clearly confirmed by XPS and XRD measurements that all the samples exhibited structural phase transitions into Mn_2O_3 phases, as observed in Fig. 2e and S1.† Note that TEM examinations also confirmed the presence of C-PHNTs with high crystalline Mn_2O_3 contents (Fig. 2d). This result implies that the treatment temperature plays an important role in determining the pore size as well as the crystal structure. Thus, these findings suggest that although the exact mechanism for the formation of the porous-wall structure remains unclear, the generation of porous void spaces is attributed to the structural transition and growth of grain aggregates induced by Ostwald ripening processes during the microwave process.²⁴ To address whether our hybrid approach based on hierarchical architecture design can overcome existing challenges, we performed electrochemical measurements with commercial Mn_2O_3 , C-PHNT 400, C-PHNT 500, and C-PHNT 600

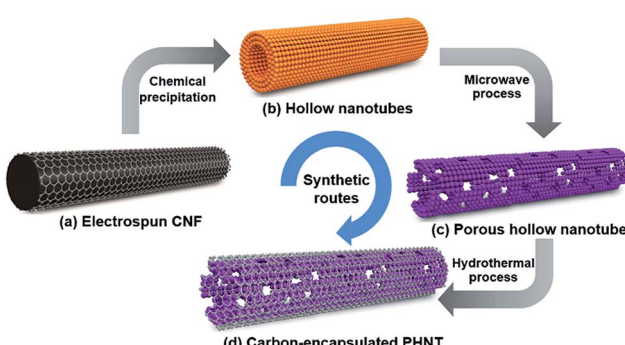


Fig. 1 Schematic illustration of synthetic routes for C-PHNTs. (a) Electrospun CNFs as template materials. (b) Hollow manganese oxide nanotubes fabricated by a chemical precipitation method. (c) PHNTs obtained through the microwave process. (d) C-PHNTs with well-defined void spaces prepared by a hydrothermal method.

samples. Fig. 3a summarizes the cycling stability of the charge–discharge capacities evaluated at a current density of 100 mA g^{-1} up to 100 cycles in the potential range of 0–3 V (*versus* Li/Li⁺). For comparison, a commercial Mn₂O₃ electrode without a porous hollow structure and a carbon layer was also prepared and measured. The first specific charge and discharge capacities were 950 and 1650 mA h g^{-1} for C-PHNT 400, 1100 and 1781 mA h g^{-1} for C-PHNT 500, and 1301 and 1903 mA h g^{-1} for C-PHNT 600, respectively, which are much higher than the values for commercial Mn₂O₃ (644 and 1550 mA h g^{-1} , respectively); the voltage profiles of the electrodes are also presented in Fig. S4†. Note that the first discharge capacities of all electrodes are higher compared to the theoretical value (*i.e.*, 1018 mA h g^{-1}).^{25–27} These excess capacities could be attributed to the direct formation of solid electrolyte interface (SEI) layers with the ability to store charges *via* interfacial charging at the metal/Li₂O interface.^{28–30} It has been well known that the SEI layers can be commonly formed within the first few cycles due to the reductive decomposition of electrolyte components on the electrode surface.^{31–33} Thus, in general, large initial irreversible capacity losses result from such SEI layers serving as a passivation layer on the surface of anode materials as shown in Fig. 3a and S4.†^{28–33} Nevertheless, C-PHNT

600 exhibited a high coulombic efficiency of 68.3% compared to the commercial Mn₂O₃ (41.5%), C-PHNT 400 (57.5%), C-PHNT 500 (61.7%), and the previously reported Mn₂O₃-based anode materials.^{26,30,31} Moreover, the C-PHNT anode materials reached a coulombic efficiency of near 100% after 3 cycles. These results suggest that the carbon-encapsulated porous hollow structure plays an important role in determining the battery performance during the initial cycling. Although a detailed understanding of the origin of the initial capacity loss is still lacking because of the complexity of a formulated electrode structure, many groups reported that the carbon coating or encapsulation layers with the high electronic conductivity around anode materials can mitigate the initial large capacity loss.^{9,10,34,35} Furthermore, as expected, the obtained C-PHNT anode materials exhibited improved cycling stability, indicating that the well-defined pore and interior void spaces can provide efficient accommodation for volume expansion.

While the commercial Mn₂O₃ exhibited a rapid drop of the specific capacity to 42 mA h g^{-1} after 100 cycles, the C-PHNT samples exhibited better stability and higher specific capacity retention up to 100 cycles. Remarkably, the C-PHNT 600 anode material with a well-defined porous structure exhibited

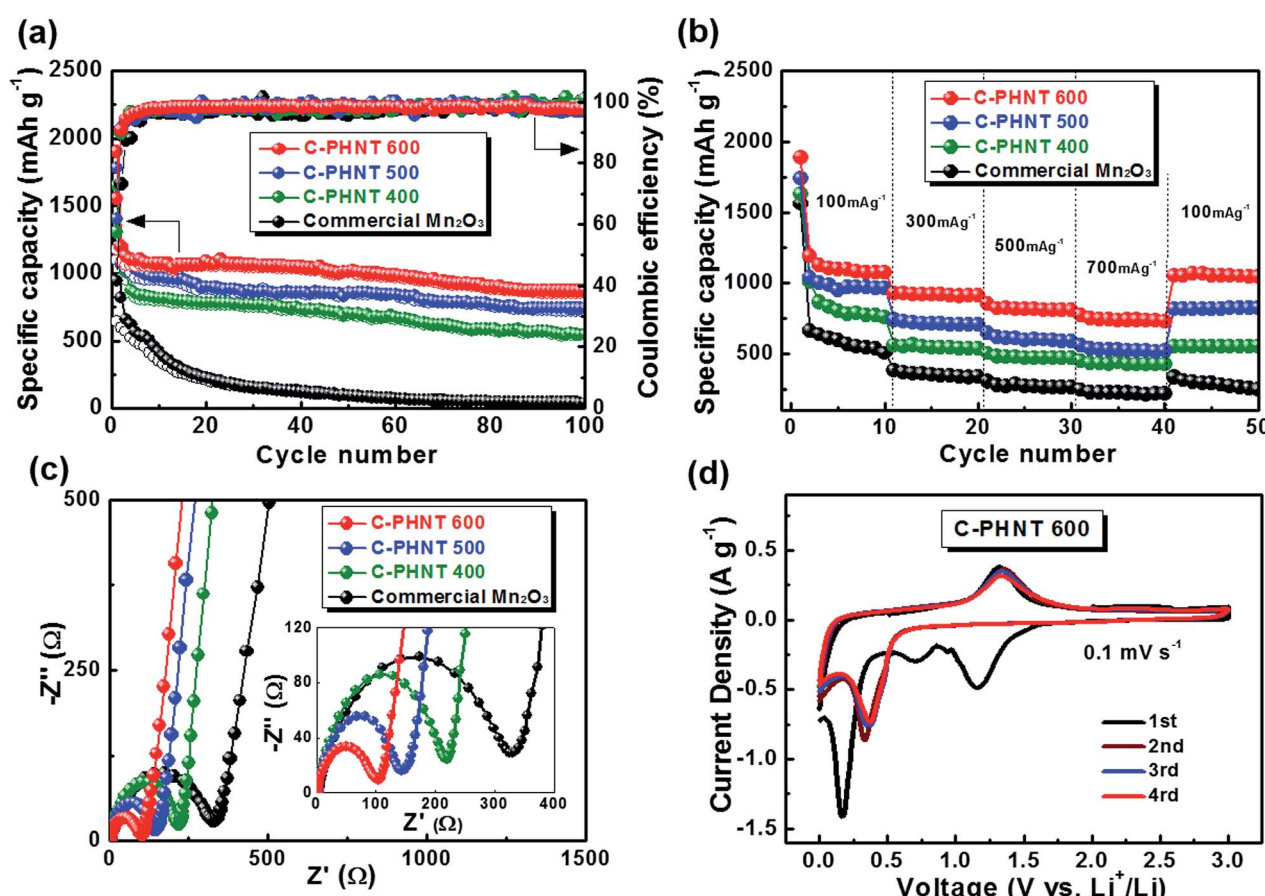


Fig. 3 Electrochemical characteristics of C-PHNT structured electrodes. (a) The cycling stability of the charge–discharge capacities of commercial Mn₂O₃, C-PHNT 400, C-PHNT 500, and C-PHNT 600 at current densities of 100 mA g^{-1} up to 100 cycles. (b) The high-rate performance at current densities of 100, 300, 500, 700, and 100 mA g^{-1} . (c) Nyquist plots in the frequency range of 10^5 to 10^{-2} Hz before the charge–discharge tests. (d) CV curves of C-PHNT 600 in the potential range of 0.0–3.0 V (*versus* Li/Li⁺) at a scan rate of 0.1 mV s^{-1} .

impressive cycling stability with a specific capacity of 875 mA h g⁻¹ after 100 cycles, which is comparable to the theoretical value, even though there is an initial irreversible capacity loss. It should be noted that this capacity is 20 times greater than the value obtained from the commercial Mn₂O₃ and the highest value reported to date for manganese-oxide-based anode materials with various geometries, as summarized in Table S1.^{†,25-32} The morphology and the structure of the C-PHNT 600 remain well after 100 cycles (Fig. S6†), indicating that the porous hollow structure and a carbon layer are beneficial to relax the volume expansion during the insertion/extraction cycling.

Moreover, the C-PHNT 600 anodes exhibited excellent high-rate performance, as observed in Fig. 3b. That is, their specific capacities (in the 10th cycle, respectively, as observed in Fig. 3b) varied from 1076 to 729 mA h g⁻¹ with an increase in current densities from 100 to 700 mA g⁻¹ and were then recovered to 1053 mA h g⁻¹, 98% of the original specific capacity, when the current density returned to 100 mA g⁻¹ with favourable Li-ion diffusion *via* the porous-wall structure. Furthermore, the C-PHNT 600 showed the high specific capacity of 633 mA h g⁻¹ after 100 cycles at a high current density of 700 mA g⁻¹ (Fig. S7†), indicating that the optimized C-PHNT can be used for applications of LIBs where fast discharge/charge is required.

In contrast, the other anode materials exhibited a sudden decrease in the reversible capacities with increasing current densities, indicating the poor high-rate performances. Notably, the outstanding rate performance of C-PHNT 600 is among the best compared with the previously reported results for Mn₂O₃-based anode materials (Fig. S5†).^{18,27-30} We believe that the observed specific capacity combined with excellent cycling stability and high-rate performances are mainly attributed to the unique hierarchical architecture with a well-defined carbon-encapsulated porous-wall and hollow-tube structure, allowing favourable Li-ion diffusion and electron transport as well as an effective accommodation for volume expansion of manganese oxides.

It should be further noted that the charge transfer kinetics, affecting the high-rate and cycling stability, is an important factor to consider in designing high-performance LIBs from the viewpoint of the electrode material structure. To verify that our unique C-PHNT structured electrodes were beneficial for improving charge transfer kinetics, electrochemical impedance spectroscopy (EIS) measurements were performed using fresh cells. Fig. 3c presents Nyquist plots of the commercial Mn₂O₃, C-PHNT 400, C-PHNT 500, and C-PHNT 600 at open-circuit potential. The semicircle in the medium-frequency range corresponds to the charge transfer impedance (R_{ct}) at the electrode/electrolyte interface and the inclined line along an imaginary axis in the low-frequency range represents the Warburg impedance attributed to the Li-ion diffusion process within the electrodes.^{32,33} The C-PHNT 600 exhibits the lowest R_{ct} with low Warburg impedance compared with the other electrode materials because of the hierarchical porous-wall and hollow-tube morphology, indicating the enhanced charge transfer kinetics, namely, indicative of improved electronic conductivity, fast ion diffusion, and a short ion diffusion pathway. It is evident that the C-PHNT structure has superior

advantages both in Li-ion and electron charge transport, which is consistent with the significantly improved high-rate and cycling stability results observed in Fig. 3a and b. These results suggest that the unique structure of the designed electrode materials, consisting of a hierarchical porous-wall and hollow-tube morphology geometrically encapsulated by carbon layers, can facilitate the favourable Li-ion diffusion and fast charge transfer and can also allow the improved quality of the electrode/electrolyte contact as well as the contact area.^{2,18,25,26,28}

To further understand the electrochemical features of hybrid C-PHNT structured anodes based on manganese oxide, cyclic voltammogram (CV) measurements were performed with a representative C-PHNT 600 sample using a potentiostat/galvanostat in the potential range of 0–3 V (*versus* Li/Li⁺) at a scan rate of 0.1 mV s⁻¹. The selection of the potential range is critical in realizing electrochemical performance. In addition, a slow scan rate was used to study the specific reaction mechanism during the electrochemical reaction in LIBs. The first CV curve clearly reveals three reduction peaks (Li insertion) and two oxidation peaks (Li extraction) as observed in Fig. 3d, which is a typical feature of Mn₂O₃. The main reduction peaks at 1.15 and 0.16 V in the first cathodic process correspond to the reduction of Mn³⁺ to Mn²⁺ and the further reduction of Mn²⁺ to Mn⁰, respectively.²⁶ However, the minor peak at approximately 0.71 V can be attributed to the formation of an irreversible solid-electrolyte interface (SEI) layer on the carbon encapsulation layer and conducting materials.³⁶ During the first anodic process, the two peaks at 1.31 and 2.41 V can be attributed to the oxidation of Mn⁰ to Mn²⁺ and Mn²⁺ to Mn³⁺, respectively. Furthermore, it was observed that in the second process, the main cathodic peak was shifted to approximately 0.33 V, which was attributed to the formation of irreversible processes such as the formation of an SEI layer and amorphous Li₂O phase in the first cathodic process.^{26,27,37} After the third and fourth processes, the peak current and integrated area mostly overlapped, indicating the excellent reversibility of the electrochemical reaction. Therefore, the electrochemical conversion reaction of C-PHNT 600 includes the following steps given by the reactions:^{28-30,37}



These results are in good agreement with the discharge-charge curves of C-PHNT 600 in Fig. S4d.† In the first discharge curve, the voltage drops from 3.0 V to a plateau at 1.15 V, which could be related to the reduction of Mn₂O₃ to Mn₃O₄, as expressed in eqn (1). Then, a second voltage drop occurs from 1.15 to 0.3 V, which could be associated with the reduction of Mn₃O₄ to MnO (eqn (2)). Finally, the voltage drops from 0.3 to 0 V, which is attributed to the reduction of MnO to Mn (eqn (3)). In the subsequent discharge curves, the discharging plateaus of PHNF/C 600 were up-shifted to 0.51 V. This phenomenon can be

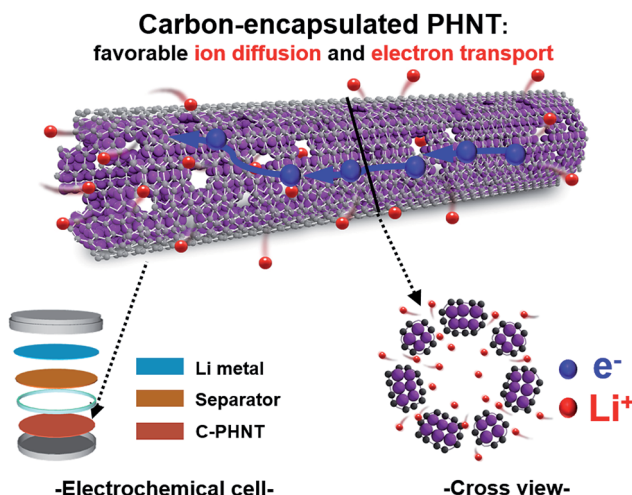


Fig. 4 Schematic of cell configuration and charge transport in a carbon-encapsulated PHNT anode.

explained by the irreversible Li-ion insertion reaction including the formation of an SEI layer and LiO_2 phases.

Here, we propose remarkable lithium storage properties for our uniquely designed anode structures with multiple advantages to elucidate the observed high specific capacity combined with excellent stability and high-rate capacity (Fig. 4). The unique carbon-encapsulated structures with well-defined pore and interior void spaces can enable improved cycling stability with high specific capacity because they provide not only enough spaces to synergistically accommodate the volume expansion but also high surface area, increasing the active sites between the electrolyte and anode material. The porous surface morphological properties of the anode materials are more favourable for Li-ion diffusion at high current densities because of the shorter Li-ion diffusion routes, allowing for outstanding high-rate performances. Additionally, the presence of a carbon encapsulation layer acting as a physical buffer layer can effectively provide more stable cycling stability because of the prevention of the structural breakdown during the Li-ion insertion/extraction. It is noted that the PHNT without carbon encapsulation layers exhibited a relatively poor cycling stability (645 mA h g^{-1} after 100 cycles) compared with that of the C-PHNT 600, as observed in Fig. S8.[†] Nevertheless, the PHNT without carbon encapsulation layers exhibited high specific capacity compared with the commercial Mn_2O_3 . In addition, the EIS examinations in Fig. S9[†] indicate that the carbon layer could contribute not only to enhance the charge transfer kinetics but also to prevent structural volume expansion.

Conclusions

We designed and successfully synthesized novel hierarchical carbon-encapsulated PHNTs by combining a simple microwave process with a hydrothermal method. The optimized C-PHNT 600 anode materials exhibited outstanding electrochemical performances with high reversible specific capacities with the best cycling stability (875 mA h g^{-1} capacity retention up to

100 cycles) and superb high-rate performance (729 mA h g^{-1} at 700 mA g^{-1}) compared with Mn_2O_3 -based anode materials reported previously as well as commercial Mn_2O_3 , C-PHNT 400, and C-PHNT 500. The excellent electrochemical features of the C-PHNT structured anodes can be explained by the combined effects of the hierarchical porous hollow geometries and carbon encapsulation layers on the structural stability and charge transport kinetics behaviour. This approach is expected to be an attractive potential strategy for other high-performance applications such as energy storage devices, sensors, and electrocatalysts.

Acknowledgements

This work was supported by the Industrial Fundamental Technology Development Program (10052745, Development of nano-sized (100 nm) manganese ceramic material for high voltage pseudo-capacitor) funded by the Ministry of Trade, Industry and Energy (MOTIE) of Korea.

References

- V. Etacheri, R. Marom, R. Elazari, G. Salitra and D. Aurbach, *Energy Environ. Sci.*, 2011, **4**, 3243–3262.
- L. Ji, Z. Lin, M. Alcoutlabi and X. Zhang, *Energy Environ. Sci.*, 2011, **4**, 2682–2699.
- M. Armand and J. M. Tarascon, *Nature*, 2008, **451**, 652–657.
- P. G. Bruce, B. Scrosati and J. M. Tarascon, *Angew. Chem., Int. Ed.*, 2008, **47**, 2930–2946.
- H. Li, Z. Wang, L. Chen and X. Huang, *Adv. Mater.*, 2009, **21**, 4593–4607.
- B. Simo, S. Flandrois, K. Guerin, A. Fevrier-Bouvier, I. Teulat and P. Biensan, *J. Power Sources*, 1999, **81–82**, 312–316.
- F. Cheng, J. Liang, Z. Tao and J. Chen, *Adv. Mater.*, 2011, **23**, 1695–1715.
- C.-M. Park, J.-H. Kim, H. Kim and H.-J. Sohn, *Chem. Soc. Rev.*, 2010, **39**, 3115–3141.
- Z. Wu, B. Li, Y. Xue, J. Li, Y. Zhang and F. Gao, *J. Mater. Chem. A*, 2015, **3**, 19445–19454.
- S. Yu, J.-W. Jung and I.-D. Kim, *Nanoscale*, 2015, **7**, 11945–11950.
- S. Liang, J. Zhou, J. Liu, A. Pan, Y. Tang, T. Chen and G. Fang, *CrystEngComm*, 2013, **15**, 4998–5002.
- G.-H. An, S.-J. Kim, K.-W. Park and H.-J. Ahn, *Electrochim. Solid-State Lett.*, 2014, **3**, M21–M23.
- G.-H. An and H.-J. Ahn, *J. Power Sources*, 2014, **272**, 828–836.
- G. Zhang, H. Bin Wu, H. E. Hoster and X. W. Lou, *Energy Environ. Sci.*, 2014, **7**, 302–305.
- D. Kong, H. He, Q. Song, B. Wang, W. Lv, Q.-H. Yang and L. Zhi, *Energy Environ. Sci.*, 2014, **7**, 3320–3325.
- L. Zhang, H. B. Wu, Y. Yan, X. Wang and X. W. Lou, *Energy Environ. Sci.*, 2014, **7**, 3302–3306.
- Y. Chen, X. Li, X. Zhou, H. Yao, H. Huang, Y.-W. Maiad and L. Zhou, *Energy Environ. Sci.*, 2014, **7**, 2689–2696.
- H. B. Lin, H. B. Rong, W. Z. Huang, Y. H. Liao, L. D. Xing, M. Q. Xu, X. P. Li and W. S. Li, *J. Mater. Chem. A*, 2014, **2**, 14189–14194.

- 19 H. B. Wu, J. S. Chen, H. H. Hng and X. W. Lou, *Nanoscale*, 2012, **4**, 2526–2542.
- 20 R. Mukherjee, R. Krishnan, T.-M. Lu and N. Koratkar, *Nano Energy*, 2012, **1**, 518–533.
- 21 Z. Lei, J. Zhang and X. S. Zhao, *J. Mater. Chem.*, 2012, **22**, 153–160.
- 22 Y. Luo, J. Jiang, W. Zhou, H. Yang, J. Luo, X. Qi, H. Zhang, D. Y. W. Yu, C. M. Li and T. Yu, *J. Mater. Chem.*, 2012, **22**, 8634–8640.
- 23 S. Ardizzone, C. L. Bianchi and D. Tirelli, *Colloids Surf., A*, 1998, **134**, 305–312.
- 24 A. Baldan, *J. Mater. Sci.*, 2002, **37**, 2171–2202.
- 25 Y. Deng, Z. Li, Z. Shi, H. Xu, F. Peng and G. Chen, *RSC Adv.*, 2012, **2**, 4645–4647.
- 26 Y. Zhang, Y. Yan, X. Wang, G. Li, D. Deng, L. Jiang, C. Shu and C. Wang, *Chem.-Eur. J.*, 2014, **20**, 6126–6130.
- 27 X. Zhang, Y. Qian, Y. Zhu and K. Tang, *Nanoscale*, 2014, **6**, 1725–1731.
- 28 L. Chang, L. Mai, X. Xu, Q. An, Y. Zhao, D. Wang and X. Feng, *RSC Adv.*, 2013, **3**, 1947–1952.
- 29 L. Hu, Y. Sun, F. Zhang and Q. Chen, *J. Alloys Compd.*, 2013, **576**, 86–92.
- 30 Y. Dai, H. Jiang, Y. Hu and C. Li, *RSC Adv.*, 2013, **3**, 19778–19781.
- 31 Y. Cai, S. Liu, X. Yin, Q. Hao, M. Zhang and T. Wang, *Phys. E*, 2010, **43**, 70–75.
- 32 S. Chen, F. Liu, Q. Xiang, X. Feng and G. Qiu, *Electrochim. Acta*, 2013, **106**, 360–371.
- 33 S. M. Abbasa, S. T. Hussain, S. Ali, N. Ahmad, N. Ali and K. S. Munawar, *Electrochim. Acta*, 2013, **105**, 481–488.
- 34 J. Shin, W.-H. Ryu, K.-S. Park and I.-D. Kim, *ACS Nano*, 2013, **8**, 7330–7341.
- 35 J. Shin, K. Park, W.-H. Ryu, J.-W. Jung and I.-D. Kim, *Nanoscale*, 2014, **6**, 12718–12726.
- 36 L. Wang, D. Deng, L. C. Lev and S. Ng, *J. Power Sources*, 2014, **265**, 140–148.
- 37 Y. Qiu, G.-L. Xu, K. Yan, H. Sun, J. Xiao, S. Yang, S.-G. Sun, L. Jin and H. Deng, *J. Mater. Chem.*, 2011, **21**, 6346–6353.